1496 *KSME International Journal, Vol. 17 No. 10, pp. 1496~1506, 2003*

# The Role of S-Shape Mapping Functions in the SIMP Approach for Topology Optimization

**Gil Ho Yoon, Yoon Young Kim***

*School of Mechanical and Aerospace Engineering, and National Creative Research Initiatives Center for Multiscale Design Seoul National University, Shinlim-Dong, San 56-1, Kwanak-Gu, Seoul 151-742, Korea*

The SIMP (solid isotropic material with penalization) approach is perhaps the most popular density variable relaxation method in topology optimization. This method has been very successful in many applications, but the optimization solution convergence can be improved when new variables, not the direct density variables, are used as the design variables. In this work, we newly propose S-shape functions mapping the original density variables nonlinearly to new design variables. The main role of S-shape function is to push intermediate densities to either lower or upper bounds. In particular, this method works well with nonlinear mathematical programming methods. A method of feasible directions is chosen as a nonlinear mathematical programming method in order to show the effects of the S-shape scaling function on the solution convergence.

**Key Words :** Topology Optimization, S-Shape Function, Nonlinear Programming

## 1. Introduction

Since the work by Bendsøe and Kikuchi (1988) for topology optimization, the interest in topology optimization has dramatically grown and been used in many engineering areas. See Bendsoe and Sigmund (2003). In many topology optimization problems, optimality criteria methods have been popular as an efficient optimizer, but there has been a growing interest in using nonlinear mathematical programming (NLP) methods. One motivation to adopt mathematical programming methods is to deal more effectively with complicated objective functions, multiple constraints, and others. For instance, SLP (sequential linear programming) was used by Sigmund (1997), Duysinx (1997), Yang et al.(1994), Nishiwaki et al.(1998), Fujii and Kikuchi (2000), and Yang and Chuang (1994). The motivation of this work is to find a method which can significantly improve the convergence speed of the NLP for topology optimization problems.

In topology optimization, intermediate values of density design variables must be avoided to get clear images of optimized structures. The most popular method in the topology optimization community is the SIMP (solid isotropic material with penalization) method (Sigmund and Petersson, 1998 ; Zhou and Rozvany, 1991), which is known to yield quite satisfactory results if the penalization parameter is chosen properly. (See Bendsøe and Sigmund, 1999 for the role of the penalization parameter.) Nonetheless, the convergence of topology optimization by mathematical programming may be substantially enhanced if intermediate densities appearing during optimization iterations are controlled effectively. The objective of this work is to present a new method to handle intermediate densities better and thus to accelerate solution convergence. In this work, we

* Corresponding Author,
**E-mail** : yykim@snu.ac.kr
**TEL** : +82-2-880-7154; **FAX** : +82-2-872-5431
School of Mechanical and Aerospace Engineering, and National Creative Research Initiatives Center for Multiscale Design Seoul National University, Shinlim-Dong, San 56-1, Kwanak-Gu, Seoul 151-742, Korea. (Manuscript **Received** April 15, 2003; **Revised** June 9, 2003)

employ a method of feasible directions (MFD) (Vanderplaats, 1984 ; Vanderplaats 1999 ; Arora, 1989) as a nonlinear mathematical programming method ; we choose this method because it consists of typical procedures such as the direction finding step and the one-dimensional search step.

When the SIMP method is employed, the stiffness of an elastic body behaves as $\rho_e^{\mu}$ where $\rho_e$ $(0<\rho_e\leq 1)$ is the element density defined by the design variable, and $\mu$ is the penalization factor (in the present work, we use $\mu=3$ unless stated otherwise). In the case of compliance minimization problems, the objective sensitivity is proportional to the stiffness sensitivity that behaves simply as $\rho_e^{\mu-1}$. Since the stiffness sensitivity in the SIMP model monotonically increases as $\rho_e$ grows from 0 to 1, the maximum stiffness sensitivity occurs at $\rho_e=1$. However, it is desirable to have higher sensitivities near intermediate densities ($\rho_e=0.5$), since intermediate densities should be avoided in final optimized results. This motivates the modification of the stiffness sensitivity field such that the resulting sensitivity field has higher values near $\rho_e=0.5$.

The straightforward multiplication of the objective sensitivity field by some nonlinear functions may work, but it lacks any theoretical justification. Instead, we propose to change design variables ; the stiffness sensitivities with respect to new design variables have the desired sensitivity field near $\rho_e=0.5$. To achieve this goal, we propose an S-shape function mapping from the original density design variables to new design variables. Because the S-shape function scales the original design variables nonlinearly, this function will be called the scaling function. The effect of using the new design variables in topology optimization is equivalent to modifying the sensitivity field formulated by the direct density variables.

A similar S-shape function was introduced by Kim and Yoon (2000) in topology optimization. The S-shape function was employed for multiscale multiresolution topology optimization where its primary use was to eliminate the side constraints imposed on density variables. Later, Poulsen (2000) employed a similar S-shape function for the same purpose. In the present work, however, a new S-shape function is designed in order to change the sensitivity field, not to eliminate side constraints. Indeed, the upper and lower bounds for new design variables are exactly the same as those of the density design variables.

The main effect of using the S-shape function in MFD manifests itself in one-dimensional search ; this will be clearly seen by a model problem as well as actual topology optimization problems. Another effect is to reduce substantially the magnitude of the components of the search direction vector when the corresponding design variables approach the lower or upper bound. In this case, the search direction modification scheme can be employed (see Vanderplaats, 1984 ; Vanderplaats, 1999) so that the next design iteration can be focused on design variables that are not close to the lower or upper bound. To find an appropriate scaling function, some requirements that nonlinear scaling functions must satisfy are also carefully investigated.

## 2. Topology Optimization Problem Statement

In this work, we will be mainly concerned with minimum compliance problems for two- and three-dimensional isotropic linear elastic structures in Bendsøe and Kikuchi (1988), Bendsøe (1995), Hassani and Hinton (1998a-c). Considering a discretized finite element model of an elastic structure, the topology optimization problem may be stated as

Minimize

$$L(\boldsymbol{\rho})=\boldsymbol{U}^T(\boldsymbol{\rho})\,\boldsymbol{F}=\boldsymbol{U}^T(\boldsymbol{\rho})\,\boldsymbol{K}(\boldsymbol{\rho})\,\boldsymbol{U}(\boldsymbol{\rho}) \quad (1)$$

subject to

$$H(\boldsymbol{\rho})=\sum_{e=1}^{N} m_e-M_0=\sum_{e=1}^{N}\rho_e v_e-M_0\leq 0 \quad (2)$$

with

$$\boldsymbol{\rho}^T=\{\rho_e\}=\{\rho_1,\ \rho_2,\ \cdots,\ \rho_N\}$$

The compliance $L$ depends on the values of element densities $\boldsymbol{\rho}$ that are subject to the side

constraints given by

$$0<\rho_e\leq 1 \qquad (e=1, 2, 3, \cdots, N) \tag{3}$$

In Eq. (1), $\boldsymbol{K}$, $\boldsymbol{U}$ and $\boldsymbol{F}$ denote the stiffness matrix of a discretized elastic structure, the nodal displacement vector and the force vector. In Eq. (2), $M_0$ represents the upper bound of the total mass of the elastic structure where $v_e$ is the volume or area of each finite element. The element density $\rho_e$ is assumed constant within an element and $N$ denotes the total number of finite elements.

The total stiffness matrix $\boldsymbol{K}(\boldsymbol{\rho})$ of an elastic body may be given by means of element-level expressions

$$\begin{aligned}\boldsymbol{K}(\boldsymbol{\rho}) &= \sum_{e=1}^{N} \boldsymbol{K}_e(\rho_e) \\ &= \sum_{e=1}^{N} \int_{\Omega_e} \boldsymbol{B}_e^T \boldsymbol{C}(\rho_e) \boldsymbol{B}_e d\Omega\end{aligned} \tag{4}$$

The strain interpolation and constitutive matrices are denoted by $\boldsymbol{B}_e$ and $\boldsymbol{C}$ which may be found in any standard finite element textbook. To express the constitutive matrix $\boldsymbol{C}$ as a function of the element density, we employ the SIMP model (Bendsøe, 1989):

$$E=E(\rho_e)=\rho_e^{\mu} E_0 \tag{5-a}$$

$$\nu=\nu_0 \tag{5-b}$$

$$m_e=\rho_e v_e \tag{5-c}$$

where $E_0$ and $\nu_0$ are Young's modulus and Poisson's ratio of a base elastic material, respectively. The element mass $m_e$ is the product of the element density $\rho_e$ and the uniform element volume $v_e$. In the case of plane stress problems, the constitutive matrix $\boldsymbol{C}$ is written as a function of $\rho_e$ as

$$\mathbf{C}(\rho_e)=\frac{E(\rho_e)}{1-\nu^2}\begin{bmatrix} 1 & \nu & 0 \\ \nu & 1 & 0 \\ 0 & 0 & \dfrac{1-\nu}{2} \end{bmatrix} \tag{6}$$

## 3. Method of Feasible Direction as an Optimizer

As stated in Introduction, we will use the method of feasible direction (MFD) as a mathematical programming method. Unlike sequential linear programming methods, this method can deal directly with problem nonlinearity. Although MFD can effectively handle multiple constraints, we simply work here with well-know compliance minimization problems having one mass constraint. Detailed accounts of this method are well summarized by Vanderplaats (1999). In typical mathematical programming methods including MFD, the updating scheme is

$$\boldsymbol{\rho}^{new}=\boldsymbol{\rho}^{old}+\alpha \mathbf{d}^{\rho} \tag{7}$$

In MFD, the search direction $\mathbf{d}^{\rho}$ is first determined and then a scalar $\alpha$ is found by a constrained one-dimensional search.

The direction finding subproblem can be written as (see Vanderplaats, 1999)

$$\text{Minimize} \qquad \beta \tag{8-a}$$

$$\text{subject to} \quad \begin{cases} \Delta_{\rho} L^T \mathbf{d}^{\rho} \leq \beta \\ \Delta_{\rho} H^T \mathbf{d}^{\rho} \leq \beta\theta \ \text{(if } H \text{ is active)} \end{cases} \tag{8-b}$$

$$\mathbf{d}^{\rho T} \mathbf{d}^{\rho} \leq 1 \tag{8-c}$$

where $\theta$ is a push-off factor. We use the symbol $\rho$ in the gradient operator $\nabla$ and the direction vector to emphasize that the design variables are $\boldsymbol{\rho}$. The subproblem formulated as Eq. (8) can be solved either by a linear programming method or a modified conjugate gradient method. The one-dimensional constrained search may be performed by either polynomial approximation or the golden section method.

To provide the gradient information of $L$ and $H$ for the subproblem, the sensitivities of $L$ and $H$ with respect to the $e$th design variable $\rho_e$ are needed:

$$\frac{\partial L}{\partial \rho_e}=-\boldsymbol{U}_e^T \frac{\partial \boldsymbol{K}_e}{\partial \rho_e} \boldsymbol{U}_e \tag{9}$$

and

$$\frac{\partial H}{\partial \rho_e}=\frac{\partial m_e}{\partial \rho_e}=v_e \tag{10}$$

Referring to Nishiwaki et al.(1998) and Fujii and Kikuchi (2000), one can easily see that the sensitivity $\partial L/\partial \rho_e$ depends on $\partial E/\partial \rho_e$. Since the search direction $\mathbf{d}^{\rho}$ in Eq. (8) is affected by the gradient $\nabla_{\rho} L$ among others, it is worth examining

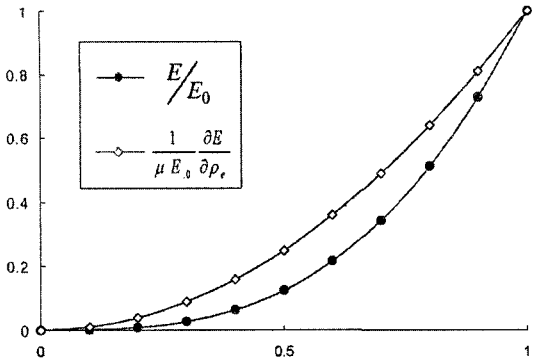


**Fig. 1** The behavior of E (Young's Modulus or the Stiffness) and $dE/d\rho_e$ as a function of $\rho_e$ (the penalization factor $\mu$ is set to 3)

the behavior of $\partial L/\partial\rho_e$ as a function of $\rho_e$. Fig. 1 plots $E(\rho_e)$ and $\partial E(\rho_e)/\partial\rho_e$ as functions of the design variable $\rho_e$. Since $\partial H/\partial\rho_e$ is independent of the design variable $\rho_e$, there is no need to examine the effect of $\nabla_\rho H$.

Although the objective sensitivity $\partial L/\partial\rho_e$ depends not only on $\partial E(\rho_e)/\partial\rho_e$ but also on $U_e$ (see Eq. (9)), some important observations can be drawn from Fig. 1. In topology optimization, intermediate densities variables should not appear in final optimized results. If the sensitivity values near $\rho_e=0.5$ were larger than those near $\rho_e=0.0$ or $\rho_e=1.0$, the faster convergence might be achieved. If this is the case, the direction vector components corresponding to intermediate density values would become larger and thus intermediate densities would move quickly towards the upper or lower bound.

In carrying out a one-dimensional search, the maximum step of $\alpha$ is determined from

$$0=\rho_e^L\le\rho_e^{old}+\alpha d_e^p\le\rho_e^U=1 \quad (e=1,\ \cdots,\ N_e) \tag{11}$$

If the maximum step is limited because some of side constraints become critical, the corresponding components of the direction vector $\mathbf{d}^p$ may be set to zero. This is equivalent to imposing $\partial L/\partial\rho_e=0$ near $\rho_e=\rho_e^L$ or $\rho_e=\rho_e^U$, giving a better search direction (see Vanderplaats, 1984; Vanderplaats, 1999). Therefore, this strategy can be strengthened, if the sensitivity is set to be very small as $\rho$ approaches either $\rho_e^L$ or $\rho_e^U$.

## 4. Introduction of an S-Shape Scaling Function

Having the motivation for the sensitivity field modification discussed in the previous section, we reconsider topology optimization using other design variables than the direct density variables. To this end, we examine the SIMP model in a general form:

$$\rho_e(x)=\Lambda(\xi_e(x))\,\rho_0 \qquad (\rho_0=1) \tag{12-a}$$

$$E_e(x)=\Theta(\xi_e(x))\,E_0 \tag{12-b}$$

Here, the design variables are $\xi_e$ and those are also restricted to satisfy the same side constraint as that for the density variables:

$$0\le\xi\le1 \tag{13}$$

In choosing the functional form of $\Lambda(\xi)$ and $\Theta(\xi)$, we also impose the following conditions

$$\Lambda(\xi=0)=0,\ \Lambda(\xi=1)=1 \tag{14-a}$$

$$\Theta(\xi=0)=0,\ \Theta(\xi=1)=1 \tag{14-b}$$

As long as $\Lambda(\xi)$ and $\Theta(\xi)$ satisfy Eq. (14), any monotonically increasing functions of $\xi$ can be candidate functions for $\Lambda(\xi)$ and $\Theta(\xi)$. However, it would be desirable that the $\rho-E$ relation can satisfy the Hashin-Shtrikmann condition (see Hashin and Shtrikman, 1963). To this end, we choose $\Theta(\xi_e)$ as

$$\Theta(\xi_e)=[\Lambda(\xi_e)]^\mu \tag{15}$$

where $\mu$ is a real number. If Eq. (15) is used, the density-stiffness relation of this model is exactly the same as the one used in the standard SIMP model:

$$E=\left(\frac{\rho}{\rho_0}\right)^\mu E_0 \tag{16}$$

In the subsequent discussions, we will call $\Lambda(\xi)$ the scaling function.

Now we consider how the sensitivity field is affected if Eqs. (12) and (15) are employed. Expressing the objective function $\hat{L}$ and $\hat{H}$ as a function of $\xi_e$

$$\hat{L}(\boldsymbol{\xi})=L(\Lambda(\boldsymbol{\xi})) \tag{17}$$

$$\hat{H}(\boldsymbol{\xi})=H(\Lambda(\boldsymbol{\xi})) \tag{18}$$

with

$$\boldsymbol{\xi}=\{\xi_e\}^T=\{\xi_1, \xi_2, \cdots, \xi_N\}^T \tag{19}$$

the sensitivities of $\hat{L}$ and $\hat{H}$ with respect to $\xi_e$ become

$$\frac{\partial \hat{L}}{\partial \xi_e}=\frac{\partial \Lambda(\xi_e)}{\partial \xi_e}\frac{\partial L}{\partial \rho_e} \tag{20}$$

and

$$\frac{\partial \hat{H}}{\partial \xi_e}=\frac{\partial \Lambda(\xi_e)}{\partial \xi_e}\frac{\partial H}{\partial \rho_e} \tag{21}$$

Eqs. (20) and (21) show that the sensitivities of the original objective function and the constraint can be controlled by $\partial\Lambda/\partial\xi_e$.

In order to reflect the observations made in the previous section in designing $\Lambda(\xi)$, we propose to use the following criteria:

I. $\Lambda(\xi=0)=0$, $\Lambda(\xi=0.5)=0.5$, $\Lambda(\xi=1)=1$ (22-a)

II. $\Lambda(\xi)+\Lambda(1-\xi)=1$ (22-b)

III. $\partial\Lambda/\partial\xi_e$ has the maximum at $\xi=0.5$ and the minimum at $\xi=0.0$ and 1.0 (22-c)

Criterion I is basically the condition given by Eq. (14) except for $\Lambda(0.5)=0.5$. Similarly Criterion II ensures that the derivative of $\Lambda(\xi)$ with respect to $\xi=0.5$ is symmetric, which emphasizes sensitivity unbiasedness towards $\xi=0.0$ or $\xi=1.0$. Criterion III states the observations made in Section 3.

With these criteria in mind, the following scaling function is proposed

$$\Lambda(\boldsymbol{\xi})=\frac{1}{1+\exp(-s(a\boldsymbol{\xi}-b))} \tag{23}$$

where $s$, $a$, $b$ are some parameters. Unless stated otherwise, we use $s=0.3$, $a=60$, $b=30$. The effects of different values of the parameter on the solution convergence will be discussed in the next section. To clarify the effects of the scaling function, we write explicitly the direction finding subproblem formulated by new design variables $\xi_e$:

$$\begin{aligned} &\text{Minimize} && \beta \\ &\text{subject to} && \begin{cases}\nabla\hat{L}^T\mathbf{d}^\xi\le\beta \\ \nabla\hat{H}^T\mathbf{d}^\xi\le\beta\theta\end{cases} \\ & && \mathbf{d}^{\xi T}\cdot\mathbf{d}^\xi\le 1 \\ & && \boldsymbol{\xi}^{new}=\boldsymbol{\xi}^{old}+\alpha\mathbf{d}^\xi \end{aligned} \tag{24}$$

## 5. Numerical Studies

In this section, we will examine the effect of the S-shape scaling function on the optimization process.

### 5.1 Model problem

To illustrate the effect of the scaling function on the performance of MFD, a simple model problem is first considered. Fig. 2 shows a system consisting of a rigid block and two elastic springs. The objective is to minimize the compliance of the system:

$$\text{Minimize} \qquad L=\frac{1}{K_T}=\frac{1}{K_1+K_2} \tag{25}$$

To simulate the topology optimization, we set

$$K_1=2K_0\rho_1^2,\ K_2=K_0\rho_2^2\ (K_0=1) \tag{26}$$

where the design variables $\rho_1$ and $\rho_2$ are subject to

$$H(\rho_1, \rho_2)=\rho_1+\rho_2\le 1 \tag{27-a}$$

$$0\le\rho_1\le 1,\ 0\le\rho_2\le 1 \tag{27-b}$$

Eq. (27-a) may be viewed as a mass constraint. If the compliance $L$ is regarded as a function of $\rho_1$ and $\rho_2$, Eq. (25) can be written as

$$\text{Minimize} \qquad L(\rho_1, \rho_2)=\frac{1}{2\rho_1^2+\rho_2^2} \tag{28}$$

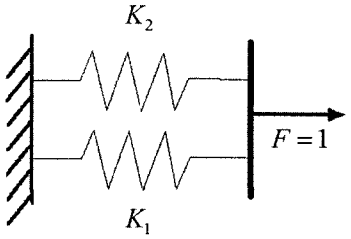


**Fig. 2** A model system consisting of a rigid block and two elastic springs

**Table 1** One iteration in MFD for a model problem in Fig. 2

| METHOD | Conventional | Present |
|---|---|---|
| Design Variables | $\rho_1$, $\rho_2$ | $\xi_1$, $\xi_2$ |
| Initial Values | $\rho^{old}=(0.5, 0.1)^T$ | $\xi^{old}=(0.5, 0.37793)^T$ $[\xi^{old}=\Lambda^{-1}(\rho^{old})]$ |
| $L^{old}$, $H^{old}$ | 1.9608, −0.4 | 1.9604, −0.4 |
| New Values | $\rho^{new}=(0.86364, 0.13636)^T$ | $\xi^{new}=(0.1783, 0.38217)^T$ $[\rho^{new}=\Lambda(\xi^{new})=(0.89292, 0.10708)]$ |
| $L^{new}$, $H^{new}$ | 0.6621, 0 | 0.62263, 0 |

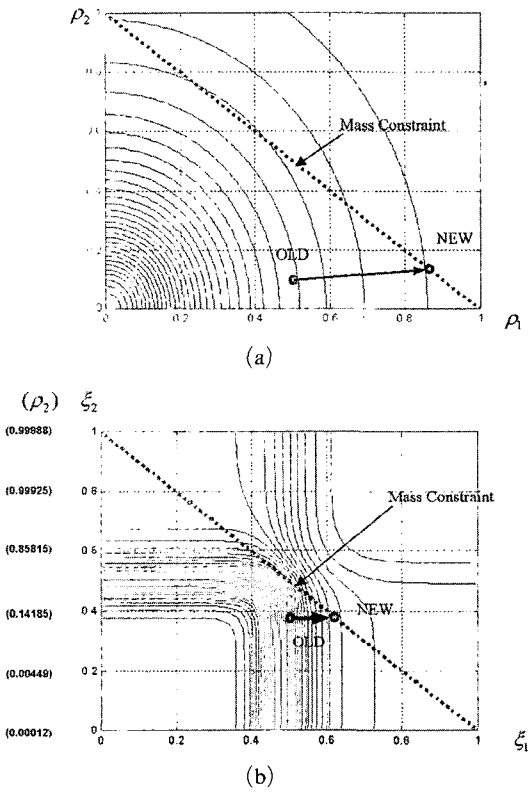


**Fig. 3** Old and new design points plotted on the contour plane for (a) $L(\rho_1, \rho_2)$ and (b) $\hat{L}$ $(\xi_1, \xi_2)$ (the design variables used for (a) and (b) are $(\rho_1, \rho_2)$ and $(\xi_1, \xi_2)$, respectively)

One can analytically find the optimal solution as $(\rho_2=1, \rho_2=0)$.

Assuming that the initial values of the design variables are $(\rho_1^{old}=0.5, \rho_2^{old}=0.1)$, equivalently, $(\xi_1^{old}=\Lambda^{-1}(\rho_1^{old})=0.5, \xi_2^{old}=\Lambda^{-1}(\rho_2^{old})=0.37793)$, we consider two optimization processes of MFD, the conventional one with $(\rho_1, \rho_2)$ and the present one with $(\xi_1, \xi_2)$. Table 1 compares the detailed one-step updating process of the conventional and the present approach in MFD and Fig. 3 plots the old and new design points by the two methods. First, we can see that the compliance by the present S-shape method is better than that by the conventional method. Second, the updated density values by the present method are closer to the lower or upper bound. The differences in these values during one step are not so significant, but the accumulated effects on solution convergence are quite significant. This will be clearly seen in the actual topology optimization process.

### 5.2 Effects of the parameters of S-shape functions

The effects of parameters, (i.e. $s$, $a$ and $b$ of S-shape functions) on solutions are also examined. Fig. 4 shows $\Lambda(\xi)$ and $\partial\Lambda(\xi)/\partial\xi$ for different values of $s$. If s becomes too small, $\partial\Lambda(\xi)/\partial\xi$ may become very small in a considerably large range of $\xi$. On the other hand, the sensitivity at $\xi=0.5$ becomes too flat if $s$ becomes too large. Therefore, no good result is expected in either extreme. Several numerical tests have suggested that the best results are obtained with $s=0.3$. (This value is also numerically tested and adopted in Kim and Yoon (2000).) However, the optimized results are not so sensitive to the choice of $a$ and $b$ (We use $a=60$, $b=30$ and $s=0.3$ for all numerical results given here.).

### 5.3 One-step update for topology optimization

Here we carry out a one-step update by MFD

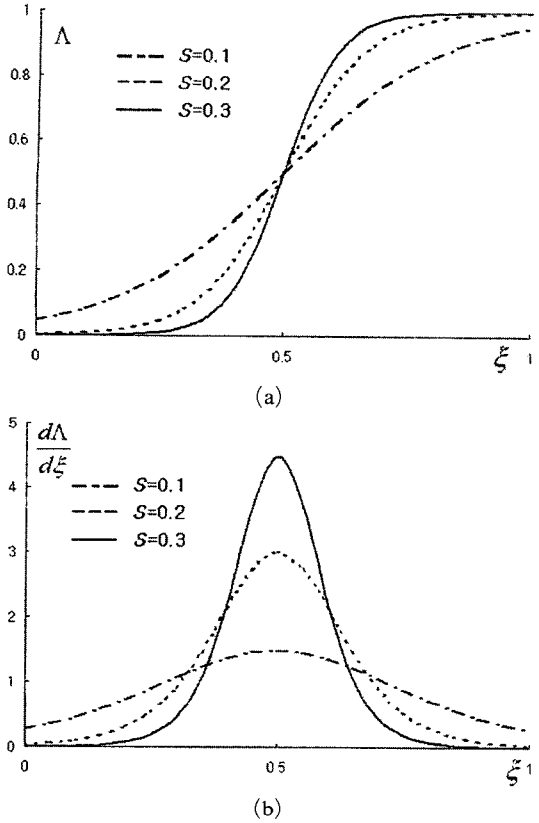


**Fig. 4** (a) S-shape scaling functions and (b) the derivative of the S-shape scaling functions for various values of $s$

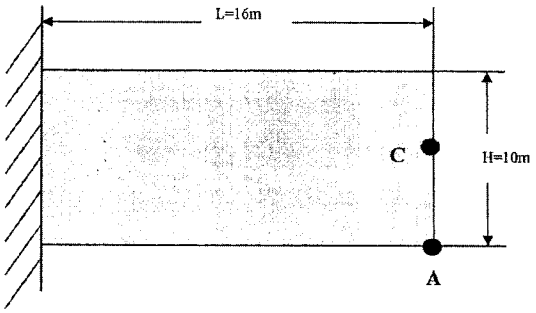


**Fig. 5** Design domain with one side clamped ($L$= 16 m, $H$=10 m, $E$=200×10$^5$ Pa, $\nu$=0.3, mass constraint=37.5% (60/160))

**Fig. 6** The density distribution at the current (old) stage

for topology optimization. The compliance minimization in consideration is illustrated in Fig. 5 where the vertical force is applied at A. The design domain is divided by 8×8 finite elements. In all numerical calculations, we use four-node bilinear finite elements and employ the filtering method (Sigmund and Petersson, 1998) to control the formation of checkerboard patterns.

To illustrate the effects of the S-shape function for the updating process, we choose a density distribution at a certain design iteration stage as a current (old) density distribution. The density values at the old stage are written on each finite element of the discretized design domain: see Table 2 for the numerical values and Fig. 6 for the corresponding image. Once $\rho_e$ ($e$=1, ⋯, $N_e$) are known at the old stage, the corresponding $\xi_e$ can be easily found using $\xi_e=\Lambda^{-1}(\rho_e)$. Therefore, we will not list the value of $\xi_e$ at the old stage. Table 3 summarizes the result obtained after a one-step iteration in MFD by the conventional and present method.

Table 3 clearly shows the advantage of the present approach working with new design variables scaled by the S-shape function. The objective value by the present method is lower than that by the conventional method. Furthermore, the number of intermediate density variables is reduced substantially by the present method (see $N(\rho_{\text{int}})$ in Table 3). To show the detailed process, the search directions ($\mathbf{d}^\rho$ and $\mathbf{d}^\xi$) by the conventional and present approach are listed in Tables 4 and 5.

The search directions $\mathbf{d}^\rho$ and $\mathbf{d}^\xi$ are tabulated in Tables 4 and 5, respectively. To obtain the results in these tables, Eqs. (8) and (24) are solved, first. Then the components of the search directions are set to zero if the corresponding design variables reach the side constraints. To see the effect of the present nonlinear scaling function,

**Table 2** The distribution of the density ($\rho_e$) (the cell location in this table stands for the element location in the design region shown in Fig. 5)

| | | | | | | | |
|---|---|---|---|---|---|---|---|
| 1 | 0.8693 | 0.6159 | 0.4086 | 0.2313 | 0.1004 | 0.0304 | 0.0108 |
| 0.5371 | 0.5127 | 0.3699 | 0.2666 | 0.187 | 0.1237 | 0.0649 | 0.0189 |
| 0.2127 | 0.2483 | 0.2204 | 0.1863 | 0.1679 | 0.1508 | 0.1116 | 0.0447 |
| 0.0772 | 0.1282 | 0.1407 | 0.1388 | 0.1443 | 0.1582 | 0.1574 | 0.1025 |
| 0.0774 | 0.1267 | 0.1341 | 0.1224 | 0.1148 | 0.1305 | 0.1789 | 0.2139 |
| 0.2131 | 0.2453 | 0.2081 | 0.1553 | 0.1087 | 0.0808 | 0.1444 | 0.4145 |
| 0.5362 | 0.5111 | 0.3666 | 0.258 | 0.1685 | 0.093 | 0.0523 | 0.7679 |
| 1 | 0.8664 | 0.6233 | 0.4399 | 0.3019 | 0.2253 | 0.2495 | 1 |

**Table 3** One iteration in MFD for the design problem depicted in Fig. 5 (the number of intermediate densities lying between 0.35 and 0.65 at the new stage is denoted by $N(\rho_{\text{int}})$

| METHOD | Conventional | Present |
|---|---|---|
| Design Variables | $\boldsymbol{\rho}$ | $\boldsymbol{\xi}$ |
| $L^{old}$, $H^{old}$ | $7.91\times10^4$, 15.33 | $7.91\times10^4$, 15.33 |
| $L^{new}$, $H^{new}$ | $1.43\times10^4$, 0 | $1.36\times10^4$, 0 |
| $N(\rho_{\text{int}})$ at new stage | 23 | 13 |

**Table 4** The search direction $\mathbf{d}^{\rho}$ at the density distribution given by Table 2 by the conventional approach (the magnitude of each cell represents the components of $\mathbf{d}^{\rho}$ at the corresponding element location in the design domain)

| | | | | | | | |
|---|---|---|---|---|---|---|---|
| 0.0000 | 0.0223 | 0.0371 | 0.0669 | 0.1360 | 0.1849 | 0.0494 | 0.0035 |
| 0.0173 | 0.0101 | 0.0158 | 0.0804 | 0.3934 | 0.7000 | 0.2828 | 0.0144 |
| 0.0115 | 0.0068 | 0.0195 | 0.0882 | 0.4329 | 1.0000 | 0.6100 | 0.0511 |
| 0.0031 | 0.0170 | 0.0444 | 0.0712 | 0.2048 | 0.7536 | 0.8338 | 0.1169 |
| 0.0030 | 0.0209 | 0.0519 | 0.0837 | 0.1198 | 0.3337 | 0.7025 | 0.1269 |
| 0.0064 | 0.0059 | 0.0167 | 0.0612 | 0.2033 | 0.2658 | 0.3784 | 0.0391 |
| 0.0089 | 0.0062 | 0.0096 | 0.024 | 0.0974 | 0.4013 | 0.0903 | 0.0086 |
| 0.0000 | 0.0179 | 0.0415 | 0.1129 | 0.3414 | 0.6377 | 0.4431 | 0.0000 |

**Table 5** The search direction $\mathbf{d}^{\xi}$ at the density distribution given by Table 2 by the present approach (compare this results with those in Table 4)

| | | | | | | | |
|---|---|---|---|---|---|---|---|
| 0.0000 | 0.0199 | 0.0688 | 0.1268 | 0.1892 | 0.1230 | 0.0110 | 0.0002 |
| 0.0338 | 0.0198 | 0.0288 | 0.1231 | 0.4677 | 0.5917 | 0.1328 | 0.0020 |
| 0.0151 | 0.0099 | 0.0262 | 0.1045 | 0.4726 | 1.0000 | 0.4711 | 0.0167 |
| 0.0017 | 0.0148 | 0.0419 | 0.0664 | 0.1974 | 0.7840 | 0.8637 | 0.0837 |
| 0.0017 | 0.0180 | 0.0471 | 0.0701 | 0.0949 | 0.2954 | 0.8066 | 0.1669 |
| 0.0084 | 0.0085 | 0.0216 | 0.0627 | 0.1534 | 0.1532 | 0.3649 | 0.0743 |
| 0.0173 | 0.0122 | 0.0174 | 0.0360 | 0.1067 | 0.2632 | 0.0345 | 0.0120 |
| 0.0000 | 0.0163 | 0.0765 | 0.2181 | 0.5637 | 0.8711 | 0.6497 | 0.0000 |

we examine the components of the search direction vectors corresponding to intermediate density values. Consider the elements at cell locations (1, 4) and (8, 4) in Table 2 that have intermediate density values of $\rho_e$=0.486, $\rho_e$=0.4339. The search direction components for these elements differ considerably depending on the method employed :

$$d^o(1, 4) = 0.0669 \; ; \; d^o(8, 4) = 0.1129$$
$$d^{\tilde{e}}(1, 4) = 0.1268 \; ; \; d^{\tilde{e}}(8, 4) = 0.2181$$

Since the magnitude of the maximum component of $\mathbf{d}^o$ and $\mathbf{d}^{\tilde{e}}$ is set to 1, the effects of the change in these components are quite significant.

### 5.4 Verification examples

To verify the convergence improvement achieved by the use of the present S-shape scaling function, several benchmark problems are considered. For the numerical implementation of MFD, the push-off factor $\theta$ is taken by 0.1. For the convergence check, we set the absolute change by 0.0001, the relative change by 0.0001 and the K-T condition by 0.001. The convergence criteria are checked over five successive iterations.

#### 5.4.1 Verification problem 1

As the first verification problem, we consider the compliance minimization problem depicted in Fig. 5 in which a vertical force of magnitude 1000 N is applied at A. The optimization results by the conventional and present approach are shown in Fig. 7. The optimization histories are also plotted in Fig. 8. The rapid convergence by the present approach is well demonstrated by this example ; the number of iterations by the present approach is only $N_{iter}$=32 while that by the conventional approach is as many as $N_{iter}$=266 for the same convergence criteria.

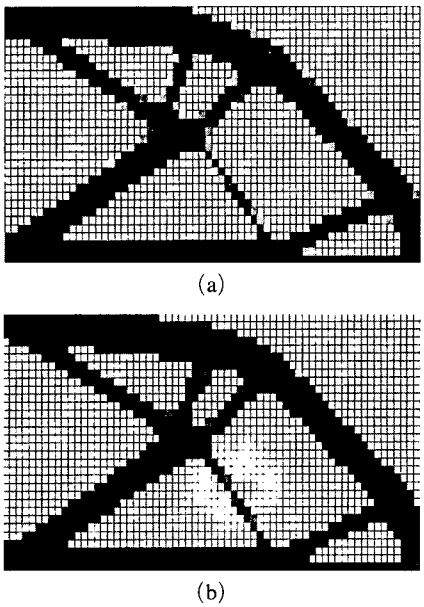

(a)

(b)

**Fig. 7** The optimized result (a) by the conventional approach ($N_{iter}$=266, $L$=144.1893, $H$=0.00394) and (b) by the present approach ($H_{iter}$=32, $L$=143.044, $H$=−0.000124) (the design domain is discretized by 2048 finite elements.)

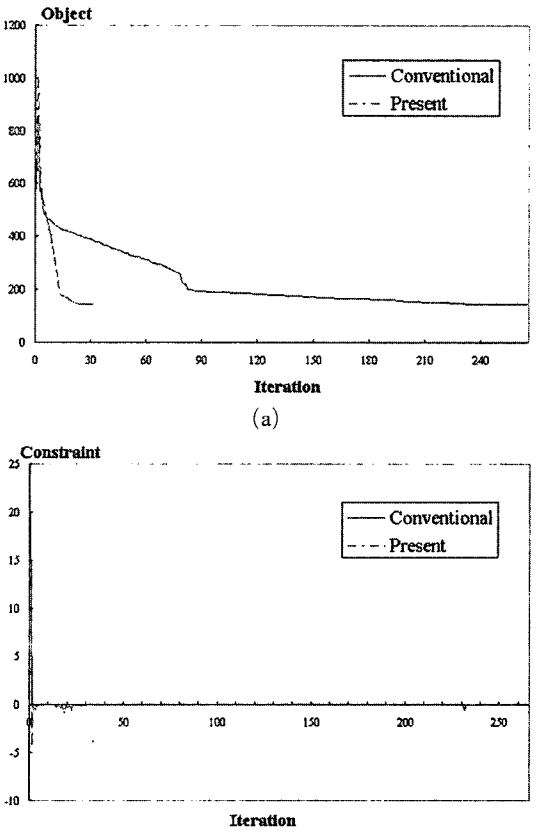


(a)

(b)

**Fig. 8** The iteration histories for the results shown in Fig. 7 : (a) the objective function and (b) the constraint function

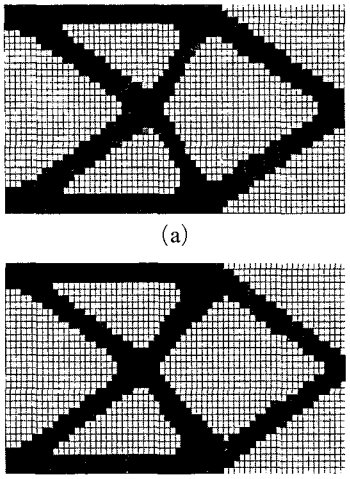

(a)

(b)

**Fig. 9** The optimized result (a) by the conventional approach ($N_{iter}$=62, $L$=130.6426, $H$=0.002975) and (b) by the present approach ($N_{iter}$=25, $L$=126.1733, $H$=−0.000096) (the design domain is discretized by 2048 finite elements.)

### 5.4.2 Verification problem 2

We now consider the compliance minimization problem for a vertical load applied at the center of the side edge denoted by C. The results are shown in Figs. 9 and 10. Again the rapid convergence is achieved by the present method working with the design variables scaled by the present S-shape function. As the initial distribution for this numerical example, we set $\rho_e$ by 0.5 for both the density method and the present method. With the different initial guesses, we have also obtained the rapid convergence by the present method.

## 6. Conclusions

The topology optimization was carried out efficiently by working with new design variables mapped from the direct density variables via an S-shape scaling function. The convergence improvement by the present method applied to nonlinear programming was illustrated by several numerical examples. The reason for the convergence speedup was investigated by studying the details of a one-step iteration process. This investigation showed that intermediate density values were effectively handled by the present S-shape function method.

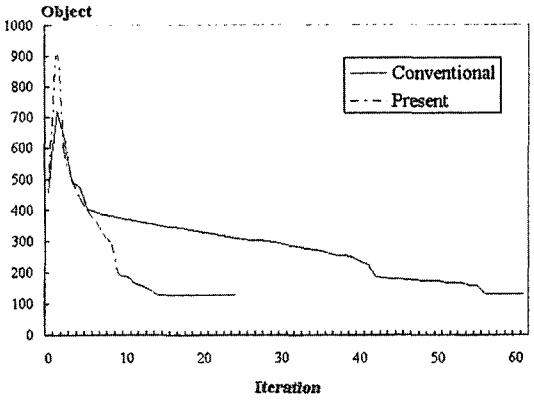


(a)

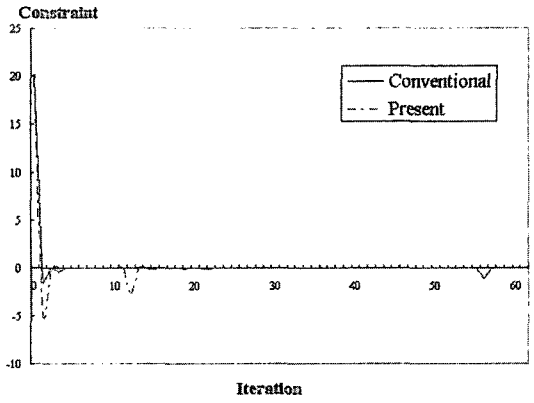


(b)

**Fig. 10** The iteration histories for the results shown in Fig. 9 : (a) the objective function and (b) the constraint function

## References

Arora, J. S., 1989, *Introduction to Optimum design*, McGRAW-HILL.

Bendsøe, M. P. and Kikuchi, N., 1988, "Generating Optimal Topologies in Structural Design Using a Homogenization Method," *Comp. Meth. Appl. Mechs. Engng.*, Vol. 20, pp. 197~224.

Bendsøe, M. P., 1995, *Optimization of Structural Topology, Shape and Material, Springer*, New York.

Bendsøe, M. P. and Sigmund, O., 1999, "Material Interpolation Schemes in Topology Optimization," *Archive of Applied Mechanics*, Vol. 69,

pp. 635~654.

Bendsøe, M. P. and Sigmund, O., 2003, *Topology Optimization Theory, Methods and Applications*, Springer-Verlag, New York.

Bendsøe, M. P., 1989, "Optimal Shape Design as a Material Distribution Problem," *Struct. Optim*, Vol. 1, pp. 193~202.

Duysinx, P., 1997, "Layout Optimization : A Mathematical Programming Approach," *DCAMM*, Vol. 540, pp. 1~30.

Fujii, D. and Kikuchi, N., 2000, "Improvement of Numerical Instabilities in Topology Optimization Using the SLP Method," *Struct. Multidisc. Optim.*, Vol. 19, pp. 113~121.

Hassani, B. and Hinton, E., 1998a, "A Review of Homogenization and Topology Optimization I-Homogenization Theory for Media with Periodic Structure," *Computers & Structures*, Vol. 69, pp. 707~717.

Hassani, B. and Hinton, E., 1998b, "A Review of Homogenization and Topology Optimization II-Analytical and Numerical Solution of Homogenization Equations," *Computers & Structures*, Vol. 69, pp. 719~738.

Hassani, B. and Hinton, E., 1998c, "A Review of Homogenization and Topology Optimization III-Topology Optimization Using Optimality Criteria," *Computers & Structures*, Vol. 69, pp. 739~756.

Hashin, Z. and Shtrikman, S., 1963, "A Variational Approach to the Theory of the Elastic Behaviour of Multiphase Materials," *Journal of the Mechanics and Physics of Solids*, Vol. 11, pp. 127~140.

Kim, Y. Y. and Yoon, G. H., 2000, "Multi-Resolution Multi-Scale Topology Optimization-A New Paradigm," *International Journal of Solids and Structures*, Vol. 37, pp. 5529~5559.

Nishiwaki, S., Frecker, M. I, Min, S. J. and Kikuchi, N., 1998, "Topology Optimization of Compliant Mechanism Using the Homogenization Method," *Int. J. Numer. Meth. Engrg.*, Vol. 42, pp. 535~560.

Sigmund, O., 1997, "On the Design of Compliant Mechanisms Using Topology Optimization," *Mechanics of Structures and Machines*, Vol. 25, No. 4, pp. 495~526.

Sigmund, O. and Petersson, J., 1998, "Numerical Instabilities in Topology Optimization : A Survey on Procedures Dealing with Checkerboards, Mesh-Dependencies and Local Minima," *Struct. Optim.*, Vol. 16, No. 1, pp. 68~75.

Poulsen, T. A., 2002, "Topology Optimization in Wavelet Space," *International Journal for Numerical Methods in Engineering*, Vol. 53, No. 3, pp. 567~582.

Vanderplaats, G. N., 1984, "ADS-A Fortran Program for Automated Design Synthesis," NASA CR 172460.

Vanderplaats, G. N., 1999, *Numerical Optimization Techniques for Engineering Design*, Colorado Springs.

Yang, R. J. and Chuang, C. H., 1994, "Optimal Topology Design Using Linear Programming," *Computers & Structures*, Vol. 52, pp. 256~275.

Zhou, M. and Rozvany, G. I. N., 1991, "The COC Algorithm, Part II : Topological, Geometry and Generalized Shape Optimization," *Comp. Meth. Appl. Mech. Engng.*, Vol. 89, pp. 197~224.